

## Lattice response at the Mott Transition in a Quasi-2D Organic Conductor

M. de Souza<sup>1</sup>, A. Brühl<sup>1</sup>, Ch. Strack<sup>1</sup>, B. Wölfl<sup>2</sup>, D. Schweitzer<sup>2</sup>, and M. Lang<sup>1</sup><sup>1</sup>Physikalisches Institut, J.W. Goethe-Universität Frankfurt(M),

FOR 412, D-60054 Frankfurt am Main, Germany and

<sup>2</sup>3. Physikalisches Institut, Universität Stuttgart, D-70550 Stuttgart, Germany

(Dated: May 25, 2019)

Discontinuous changes of the lattice parameters at the Mott metal-insulator (M I) transition are detected by high-resolution dilatometry on deuterated salts of the organic conductor  $-(BEDT-TTF)_2Cu[N(CN)_2]Br$ . The uniaxial expansivities uncover a striking and unexpected anisotropy. A second-order phase transition is observed near the end-point of the first-order transition line  $T_{MI}$ . The extraordinarily large lattice response there provides a sensitive thermodynamic probe to explore the critical behavior. The analysis yields a singular contribution with an exponent  $\sim 0.8 - 0.15$  and indicates the particular role of inhomogeneities giving rise to a broadening of the transition.

PACS numbers: 74.70.Kn, 71.30.+h, 74.25.Bt

The Mott metal-insulator (M I) transition has been the subject of intensive research for many years, see e.g. [1] for a review. Materials intensively discussed in this context include transition metal oxides, notably Cr-doped  $V_2O_3$ , and, recently, organic  $-(BEDT-TTF)_2X$  charge-transfer salts [2, 3, 4, 5]. Here BEDT-TTF (or simply ET) denotes bis(ethylenedithio)tetrathiafulvalene and X a monovalent anion. For the latter substances, an s-shaped first-order metal-insulator transition line  $T_{MI}(P)$  has been established [2, 3, 4, 5, 6], indicative of a bandwidth-controlled Mott transition [7, 8]. Pressure experiments revealed distinct anomalies at  $T_{MI}$  and suggest a second-order critical endpoint  $(P_0; T_0)$  [2, 3, 4, 5] with remarkable properties. Particularly striking was the observation of a pronounced softening of the  $c_{22}$  elastic mode [4]. In fact, a critical acoustic anomaly has been predicted recently within the compressible Hubbard model [9]. According to this and related works [10], a lattice anomaly is expected at the Mott transition in response to the softening of the electronic degrees of freedom. In addition, unconventional critical behavior at  $(P_0; T_0)$  was observed [11] and attributed to the quasi-twodimensional (quasi-2D) electronic character of the organic materials.

In this Letter we report, for the first time, the direct observation of the lattice response through the Mott transition in a  $-(ET)_2X$  organic conductor and address, via a thermodynamic probe, the criticality near  $(P_0; T_0)$ .

For the thermal expansion measurements, a high-resolution capacitive dilatometer was used, enabling the detection of length changes  $1 - 10^{-2}\text{Å}$ . Owing to the experimental difficulties posed by accomplishing high-resolution dilatometric measurements under variable pressure, use was made of the possibility of applying chemical pressure. To this end, single crystals of  $-(d8-ET)_2Cu[N(CN)_2]Br$  were synthesized with deuterium atoms replacing the protons in the terminal ethylene groups. These fully deuterated salts, referred to as d8-Br in the following, are known to be situated very

close to the M I transition [12]. First, deuterated (98%) ET molecules were prepared according to [13, 14] using multiple recrystallization for the intermediate steps. Next, single crystals were synthesized along an alternative preparation route described recently for the protonated variant h8-Br [15]. The grade of deuteration was checked by infrared reflection spectroscopy both on the deuterated ET material [16] as well as on the d8-Br single crystals [17], and found to be at least 98%. For the present study, crystals of two independently prepared batches were used: crystal # 1 (batch A 2907) and # 3 (A 2995). A preliminary account on a second crystal from batch A 2907 was given in [18]. The resistivity was studied by employing a standard four-terminal method-technique. All measurements, unless stated otherwise, were carried out after cooling through the glass-like transition at  $T_g$ , 77 K with a very low rate of  $\sim 3\text{ K/h}$  (thermal expansion) and  $\sim 6\text{ K/h}$  (resistivity) to rule out cooling-rate dependent effects, see [19].

The interlayer resistivity  $\rho$  for crystal # 1 is shown in the lower part of Fig. 1. Upon cooling,  $\rho$  passes over a maximum around 45 K, then rapidly drops and attains abruptly around 30 K. The resistivity remains metallic down to about 20 K, below which the slope sharply increases (cf. upper inset in Fig. 1) indicating the transition into an insulating state. An almost identical  $\rho$  was found for crystal # 3 and the crystal studied in [18], except for small differences around the maximum and some details in the insulating regime. For all three crystals,  $\rho$  vanishes below about 11.5 K. A zero resistivity accompanied by a tiny signature in the  $i$  data is consistent with percolative superconductivity in a minor metallic phase coexisting with an antiferromagnetic/insulating ground state for d8-Br [20], cf. the phase diagram in Fig. 3.

The main features in the resistivity have their clear correspondence in the coefficient of thermal expansion,

$\alpha = \frac{1}{T} \frac{dL}{dT}$ , also shown in Fig. 1 along the a-axis of crystal # 1. The attening of  $\alpha$  is accompanied by a huge maximum in  $\alpha(T)$  centered at a temperature

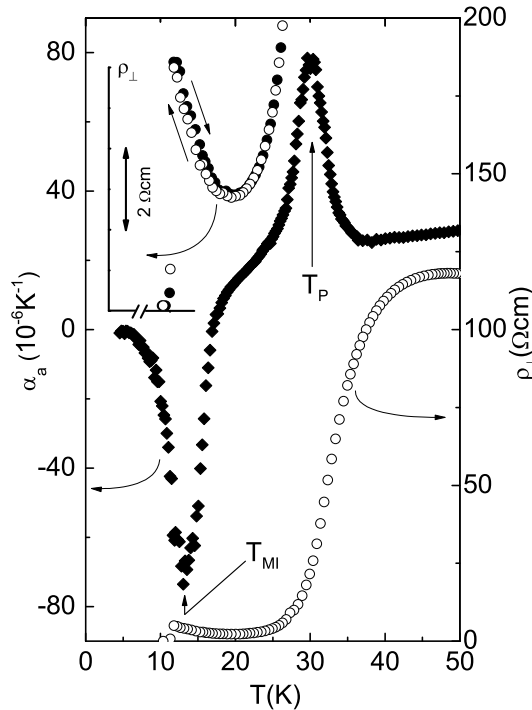


FIG. 1: Expansion coefficient along the in-plane a-axis,  $\alpha_a$ , and interlayer resistivity,  $\rho_{\perp}$ , for  $-(d8-ET)_2CuN(CN)_2Br$  crystal # 1. Upper inset shows an expansion of the low-T  $\alpha_a(T)$  data on the same T scale as used in the main panel.

$T_p$  ≈ 30 K. As will be discussed below, this effect can be assigned to a second-order phase transition. Upon further cooling,  $\alpha_a(T)$  reveals an even bigger negative peak indicating yet another phase transition. The accompanying change in  $\rho_{\perp}$  from metallic to insulating behavior suggests this peak to be due to the MI transition. A similar  $\alpha_a(T)$  behavior is observed for # 3 although with slightly reduced (~ 20%) peak anomalies at  $T_p$  and  $T_{MI}$ . More insight into the character of the transitions can be gained by looking at the relative length changes  $\Delta l_i(T) = l_i - (l_i(T) - l_i(300K))/l_i(300K)$ , ( $i = a; b; c$ ) shown in Fig.2. The dominant effects occur along the in-plane a-axis, i.e. parallel to the anion chains. Here a pronounced s-shaped anomaly is revealed at  $T_p$  which lacks any sign of hysteresis upon cooling and warming (generic features of a second-order phase transition with strong fluctuations). On further cooling through  $T_{MI}$ , the a-axis shows a rapid increase of about  $\Delta a/a = 3.5 \cdot 10^{-4}$  within a narrow temperature range, indicative of a slightly broadened first-order transition. The observation of a small but significant hysteresis of about 0.4 K (cf. lower inset Fig.2), which complies with the hysteresis in  $\rho_{\perp}(T)$  (upper inset Fig.1), confirms the first-order character. The corresponding anomalies along the b-axis are less strongly pronounced. Surprisingly, for the second in-plane c-axis, anomalous behavior in  $\Delta l_c$  can neither be discerned at

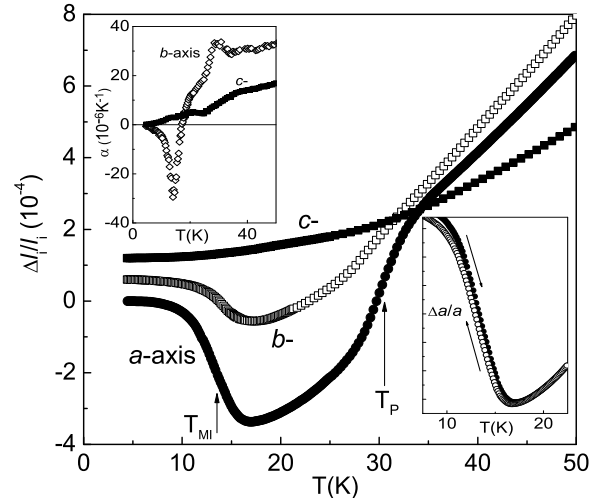


FIG. 2: Relative length changes for  $-(d8-ET)_2CuN(CN)_2Br$  crystal # 1 along the in-plane a- and c-, and out-of-plane b-axis. The data have been offset for clarity. Lower inset shows the hysteresis behavior in  $\Delta a/a$  at  $T_{MI}$  measured at very low sweeping rates of 1.5 K/h. Upper inset depicts the uniaxial expansivities along the b- and c-axis.

$T_p$  nor at  $T_{MI}$ . Yet small signatures are visible in  $\Delta l_c$  shown together with  $\Delta l_b$  in the upper inset of Fig.2.

Figure 2 reveals a clear correlation between the anomalies at  $T_p$  and  $T_{MI}$ , suggesting that both effects are intimately related to each other. Moreover, the data imply that below  $T_p$  a significant in-plane distortion a-c develops which grows down to  $T_{MI}$ , below which it becomes (at least partly) annihilated. These in-plane effects are accompanied by a considerable response along the interlayer direction. Given the quasi-2D electronic structure and a crystal lattice, which is expected to be much stiffer along the interlayer direction [21], this is a very remarkable and unexpected result: The absence of a noticeable response along the c-axis indicates that the parallel dimer-dimer interaction,  $t_{b2}$ , is not decisive for the transitions at  $T_p$  and  $T_{MI}$  (see, e.g. [8] for the definition of the hopping terms). At the same time, the dominant response in the a-axis, along which no direct dimer-dimer overlap exists, means that the diagonal interactions along the c-a directions,  $t_p$  and  $t_q$ , have to be involved in this process. The reason why these interactions leave the in-plane c-axis, which is expected to be even softer than the anion-chain a-axis [21], unaffected, and by which mechanism they influence the interlayer direction, is not obvious and demands an explanation.

Before discussing the implications of our observations, the MI-transition temperature  $T_{MI}$  is determined. As Fig.2 demonstrates, the transition is not very sharp but rather spans a range of several Kelvin (an effect which is very similar for both crystals studied here and the one explored in [18]). A broadening of signatures

in temperature-dependent measurements, as opposed to isothermal pressure sweeps, would be naturally expected given the steepness of  $T_{MI}(P)$ , cf. Fig. 3. However, the width of about 5.6 K of the  $l_a = l_a$  jump (10–90%), which transforms into a pressure interval of about 2 MPa employing a slope  $dT_{MI} = dP = 2.7 \pm 0.1 \text{ K/MPa}$  around 14 K (cf. Fig. 3), is even smaller than the transition range seen in acoustic measurements as a function of pressure [4] (cf. the hatched area in Fig. 3), but is comparable with a width of about 1.4 MPa as read off the resistivity data in [5]. These smearing effects have been attributed to a region of coexistence between insulating and metallic phases [3], as indeed recently observed via real-space imaging [23]. For lack of a well-founded procedure to treat the broadened transitions, the position of the  $(T)$  minimum is chosen as the thermodynamic transition temperature. Employing literature results on  $T_{MI}(P)$  [24], the so-derived values of  $T_{MI} = (13.5 \pm 0.8) \text{ K}$ , (# 1) and  $(14.1 \pm 0.8) \text{ K}$ , (# 3) can be used to pinpoint the position of the present d8-Br crystals on the pressure axis in the phase diagram in Fig. 3. Within the uncertainties implied in this procedure, the crystals are located very close to the critical pressure  $P_0$  as determined by the various pressure studies [2, 3, 4, 5]. The significance of this finding is threefold. First, it demonstrates that the anomaly at  $T_p$  reflects the lattice response in the immediate vicinity of  $(P_0; T_0)$ . Second, as this point is part of the  $T_{MI}(P)$  line, it provides a natural explanation for the intimate interrelation of the anomalies at  $T_p$  and  $T_{MI}$  inferred from Fig. 2. Third, it enables a determination of the entropy change associated with the MI transition near the point, where the Néel temperature  $T_N$  comes close to  $T_{MI}$ . Employing the Clausius–Clapeyron equation  $dT_{MI} = dP = V = S$  with  $V = V_I - V_M$  and  $S = S_I - S_M$ , the respective difference in volume and entropy between the insulating (I) and metallic (M) states, and using  $dT_{MI} = dP = 2.7 \pm 0.1 \text{ K/MPa}$  and  $V = V = (4.5 \pm 0.5) \cdot 10^4$ , derived from summing over the uniaxial effects in Fig. 2, one finds  $S = -0.07 \text{ Jmol}^{-1}\text{K}^{-1}$ . This small number, being only a fraction of the entropy associated with the metallic state of h8-Br at  $T = 14 \text{ K}$  of  $S = T \cdot 0.375 \text{ Jmol}^{-1}\text{K}^{-1}$ , with a Sommerfeld coefficient  $= 0.025 \text{ Jmol}^{-1}\text{K}^{-1}$  [25], indicates that the high spin entropy of the paramagnetic insulator at elevated temperatures must have been (almost) completely removed. This would be consistent with  $T_N$  coinciding with  $T_{MI}$  at this point of the phase diagram.

The extraordinarily large lattice response at  $T_p \approx T_0$ , with an  $(T)$  anomaly exceeding the background by a factor 3–4, provides a most sensitive thermodynamic probe for exploring the criticality at  $(P_0; T_0)$ . To this end, the phase transition anomaly in  $a(T)$ , shown for the crystals # 1 and # 3 in Fig. 4 on expanded scales, is analyzed in terms of a power-law behavior in the variable  $t = (T - T_0)/T_0$ . This approach is based on the proportionality of  $(T)$  to the specific heat  $C(T)$ , implying that

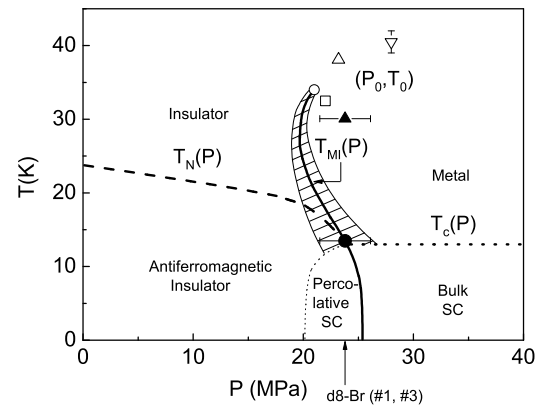


FIG. 3:  $T$ – $P$  phase diagram of  $-(ET)_2X$  including the Néel transition at  $T_N$  (dashed line) and the superconducting (SC) transition at  $T_c$  (dotted line) from [2]. Thin solid lines, delimiting the hatched area, denote positions of acoustic anomalies [4]. The middle position (thick solid line) is used here as  $T_{MI}(P)$  [24]. Closed symbols refer to anomalies at  $T_{MI}$  and  $T_p$  of the d8-Br crystals # 1 and # 3 (same positions on the scale of the figure), while open symbols denote literature results for  $(P_0; T_0)$ : (square) [2], (5) [3], (–) [4], (4) [5].

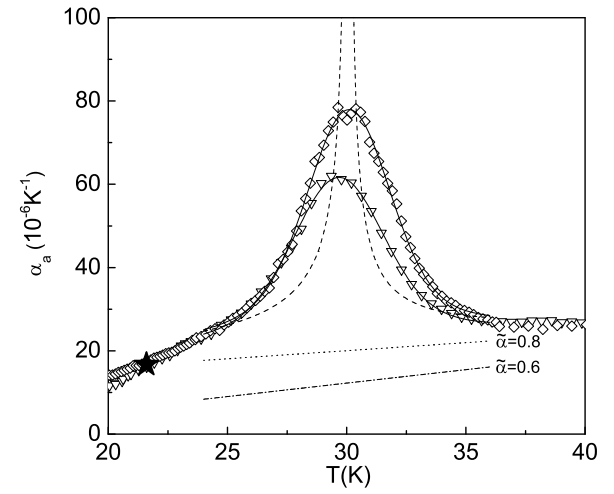


FIG. 4: Expansivity data along the  $a$ -axis for d8-Br crystals # 1 and # 3 near  $T_0$ . Solid lines are fits as described in the text with  $\alpha = 0.8$ . Dashed line corresponds to the same parameters without employing a Gaussian broadening of  $T_0$ . Dotted and dashed-dotted lines refer to background contributions obtained from fits with critical exponents given in the figure. Star marks the universal background point discussed in the text.

the same scaling laws apply at  $T_0$ , as verified by various groups, see, e.g. [26, 27].

As Fig. 4 demonstrates, the phase-transition anomalies are very similar in shape for both crystals but differ slightly in size. Before estimating the singular contribution from fits involving several parameters, some im-

portant conclusions can be drawn already from an inspection of the data sets in Fig.4. Upon approaching the maximum around 30K from both sides, the slope of  $\langle T \rangle$  increases markedly within a narrow temperature range. This behavior is distinctly different from a mean field-type transition, characterized by an approximate in- $T$  linear behavior on both sides, and provides strong evidence for a singular contribution  $\sim / \langle T \rangle \sim$  with  $\sim > 0$ . Closer to the center of the peak, however, the slope is reduced giving rise to a rounded maximum. Such broadening effects are generally encountered in the immediate vicinity of  $T_0$  and attributed to sample inhomogeneities. The rounding over a considerable temperature range here indicates that inhomogeneities are of relevance and have to be taken into account. Based on these observations, the critical exponent  $\sim$  is determined by fitting the data in the range 24 – 36K with the function  $\sim = \frac{A}{\sim} \langle T \rangle \sim + B + E \sim T$ . This equation contains the singular contribution with the amplitudes  $A^+$  and  $A^-$  for  $t > 0$  and  $t < 0$ , respectively, and a linear term. The latter comes primarily from the phonons but can also include a small non-singular electronic contribution. The smearing of the transition is accounted for by introducing a Gaussian distribution for  $T_0$  with a width

$T_0$ . To reduce the number of parameters, the linear contribution is set to be identical on both sides of  $T_0$ . In addition, the data sets of crystal # 1 and # 3 were fitted simultaneously using the same critical exponent  $\sim$ , the same ratio  $A^+ = A^-$ , and an identical linear background for both crystals. Furthermore, a constraint for the background contribution can be derived by comparing the data in Fig.4, with those of the d8-Br in [18] and h8-Br in [19]. All data sets intersect at a single point  $T = 21.2\text{K}$ ,  $\sim = 15.7 \cdot 10^6\text{K}^{-1}$ , irrespective of the presence and size of the critical contribution at  $T_0$ , indicating that this point reflects the pure background. Thus a meaningful background  $B + E \sim T$  should extrapolate to this universal point. With this additional constraint, a good fit to both data sets is obtained for  $\sim = 0.8$ ,  $A^+ = A^- = 0.79$ , and  $T_0 = 30.1\text{K}$ ,  $T_0 = 1.59\text{K}$  for # 1 and  $T_0 = 29.6\text{K}$ ,  $T_0 = 1.74\text{K}$  for # 3, cf. the solid lines through the data in Fig.4, with the straight dotted line representing the corresponding background contribution. Note that larger  $\sim$  values  $0.8 \sim 0.95$  result in a fit of similar quality, although a somewhat stronger temperature variation has to be invoked for the background to meet the universal point. On the other hand,  $\sim < 0.65$  suppresses the background in a way that it appears no longer compatible with the above criterion, cf. the background corresponding to a  $t$  with  $\sim = 0.6$  in Fig.4. The critical exponent derived here of  $\sim = 0.8 \sim 0.15$  is much larger than those of known universality classes with  $-0.12 \sim 0.14$ . In particular, it greatly contrasts with the criticality reported in [11] for pressurized  $X = \text{Cu}(\text{CN})_2\text{Cl}$ . Employing the exponent identity  $\sim + 2 \sim = 2$  [28], the exponents found there

of  $(\sim; \sim; \sim) = (2; 1; 1)$  give  $\sim = -1$ . The reason for this discrepancy is unclear but might be related to the significant broadening effects, which appear to be inherent to the present materials, and which have not been included in the analysis in [11]. The exponent found here, however, is rather close to  $\sim = 0.5$  expected for a tricritical point [29]. Such a scenario would imply a symmetry breaking associated with  $T_{MI}$  for which no evidence has yet been supplied. Interestingly, an even larger exponent  $\sim = 0.93$  was recently reported for  $\text{La}_{0.7}\text{Ca}_{0.3}\text{MnO}_3$  [27], also characterized by a strong electron-phonon coupling, showing an  $\langle T \rangle$  anomaly of comparable size and shape to the one observed here.

In summary, high-resolution dilatometry on deuterated crystals of the organic conductor  $-(\text{ET})_2\text{Cu}(\text{CN})_2\text{Br}$  reveal distinct discontinuities in the lattice parameters at the Mott metal-insulator transition  $T_{MI}$  uncovering a striking and unexpected anisotropy. The huge lattice response at the critical end-point of  $T_{MI}$  offers the possibility to explore the critical behavior via a thermodynamic probe. The analysis yields a critical exponent  $\sim = 0.8 \sim 0.15$  and indicates the particular role of inhomogeneities.

M. de Souza acknowledges financial support from the Brazilian Research Foundation CAPES.

- 
- [1] M. Imada et al., Rev. Mod. Phys. 70, 1039 (1998).
  - [2] S. Lefebvre et al., Phys. Rev. Lett. 85, 5420 (2000).
  - [3] P. Lienert et al., Phys. Rev. Lett. 91, 016401 (2003).
  - [4] D. Fournier et al., Phys. Rev. Lett. 90, 127002 (2003).
  - [5] F. K. Agawa et al., Phys. Rev. B 69, 064511 (2004).
  - [6] H. Ito et al., J. Phys. Soc. Jpn. 9, 2987 (1996).
  - [7] K. Kanoda, Hyperfine Interact. 104, 235 (1997).
  - [8] H. Kino et al., J. Phys. Soc. Jpn. 64, 2726 (1995).
  - [9] S.R. Hassan et al., Phys. Rev. Lett. 94, 036402 (2005).
  - [10] J. Merino et al., Phys. Rev. B 62, 16442 (2000).
  - [11] F. K. Agawa et al., Nature 436, 534 (2005).
  - [12] A. Kawamoto et al., Phys. Rev. B 55, 14140 (1997).
  - [13] K. Hartke et al., Chem. Ber. 113, 1898 (1980).
  - [14] M. Mizuno et al., J. Chem. Sci. Commun. 1978, 18 (1978).
  - [15] Ch. Strack et al., Phys. Rev. B 72, 054511 (2005).
  - [16] S. Gartner et al., Synth. Met. 44, 227 (1991).
  - [17] E. Griebhaber, Dissertation, University Stuttgart (2000), unpublished.
  - [18] M. Lang et al., Proceedings of the 8th Intern. Conf. on Materials and Mechanisms of Superconductivity – High Temperature Superconductors, Physica C, in press.
  - [19] J. Müller et al., Phys. Rev. B 65, 144521 (2002).
  - [20] K. Miyagawa et al., Phys. Rev. Lett. 89, 017003 (2002).
  - [21] For the related  $X = \text{Cu}(\text{NCS})_2$  salt, the uniaxial compressibilities  $k_i$  are strongly anisotropic [22] with  $k_1 : k_2 : k_3 = 1 : 0.53 : 0.17$ , and  $i = 1$  and 2 the in-plane axis perpendicular and parallel to the anion chains, respectively, and  $i = 3$  along the long axis of the ET molecules.
  - [22] D. Chasseau et al., Synth. Met. 41 – 43, 2039 (1991).
  - [23] T. Sasaki et al., Phys. Rev. Lett. 92, 227001 (2004).

- [24] Due to the finite range of phase coexistence around  $T_{M\text{ I}}$ , the comparison of the thermodynamically determined  $T_{M\text{ I}}$  values here with those derived from transport experiment [2, 3] may cause some ambiguity. We therefore refer to  $T_{M\text{ I}}(P)$  as the mean value (thick solid line in Fig. 3) of acoustic anomalies observed in pressure-dependent studies [4].
- [25] H. E. Lsinger et al., Phys. Rev. Lett. 84, 6098 (2000).
- [26] V. Pasler et al., Phys. Rev. Lett. 81, 1094 (1998).
- [27] J. A. Souza et al., Phys. Rev. Lett. 94, 207209 (2005).
- [28] L. P. Kadanoff et al., Rev. Mod. Phys. 39, 395 (1967).
- [29] K. Huang, Statistical Mechanics (Wiley, New York, 1987) 2<sup>nd</sup> ed., Chap. 17.6.